Journal of Zhejiang University-SCIENCE A (Applied Physics & Engineering)
ISSN 1673-565X (Print); ISSN 1862-1775 (Online)
www.zju.edu.cn/jzus; www.springerlink.com
E-mail: jzus@zju.edu.cn

Electromagnetic environment around a high-speed railway using analytical technique*

Yong-jian ZHI[1], Bin ZHANG[†‡2], Kai LI[3], Xiao-yan HUANG[1], You-tong FANG[1], Wen-ping CAO[4]

([1]*College of Electrical Engineering, Zhejiang University, Hangzhou 310027, China*)

([2]*State Key Lab of Fluid Power Transmission and Control, Zhejiang University, Hangzhou 310027, China*)

([3]*Department of Information Science and Electronic Engineering, Zhejiang University, Hangzhou 310027, China*)

([4]*Newcastle University, Newcastle upon Type, NE1 7RU, UK*)

[†]E-mail: zbzju@163.com

Received Sept 23, 2011; Revision accepted Sept 24, 2011; Crosschecked Sept 24, 2011

Abstract: A switched-mode unit used in electric locomotive generates a strong high frequency conducted electromagnetic interference (EMI), which radiates electromagnetic energy through railway lines. Evaluation of magnetic field using analytical technique based on contour integral is presented, in order to assess the electromagnetic environment around a high-speed railway. Actual railway multiconductor finitely long overhead lines are represented by an infinitely long single line above two-layered earth, whose characteristic is different from homogeneous earth. Owing to the constraint of the GB/T 24338-2009 and the high frequency investigated (a few MHz), only the magnetic fields are examined. The magnetic fields consist of four components: the direct wave, the ideal reflected wave or image wave, the trapped surface wave, and the lateral wave. The calculation results proved that due to the presence of the trapped surface wave, the magnetic field of the observer point on the interface is strongly influenced, when the line is on or closed to the interface.

Key words: Overhead lines, Two-layered earth, Trapped surface wave
doi:10.1631/jzus.A11GT004 **Document code:** A **CLC number:** U228.1

1 Introduction

The Beijing-Shanghai High-Speed Railway officially started operating on June 30, 2011. It is a milestone in the development of China's railway. A mass of high-powered electronic devices used in the Beijing-Shanghai High-Speed Railway System have led to the possibility of interference to the facilities in the environment, such as telecommunications lines and wireless systems, and also the possibility of affecting human health. So it is necessary to evaluate the electromagnetic environment around the railway lines. That is why the electromagnetic compatibility (EMC) standard (GB/T 24338-2009), translated from (CENELEC Standard EN 50121 (2006), has to be established. Where the electromagnetic interference (EMI) source is and how it propagate to the observer are the primary problems to be solved. The main high frequency EMI radiates electromagnetic energy from train converters. A part of the EMI is injected to the contact line, and three patterns are considered for the EMI affecting other systems: (1) as a horizontal wire antenna radiating electromagnetic energy; (2) as a multiconductor line propagating the EMI signals away from the source point; (3) as a multiconductor line leading to the crosstalk between the lines (Cozza and Demoulin, 2008).

The typical configuration of an electric railway line on the Beijing-Shanghai High-Speed Railway is sketched in Fig. 1, which depicts the electric locomotive, power supply line, and autotransformer (AT)

‡ Corresponding author

* Project supported by the National Natural Science Foundation of China (Nos. 50877070 and 51105331), and the Technological Research and Development Programs of the Ministry of Chinese Railways (Nos. 2009J006-L and 2010J011-E)

used in the power supply system. Electric energy mainly supplied to traction electric machine is regulated by a switched-mode unit, which generates a strong conducted EMI due to the fast switch on and off. The conducted EMI goes back to the overhead supply-line through a pantograph, thus imposing external interference through radiation and propagation along the supply-line. The interference mentioned-above is the secondary radiation and there is also primary radiation from the high-powered electronic devices themselves (Cozza and Demoulin, 2008).

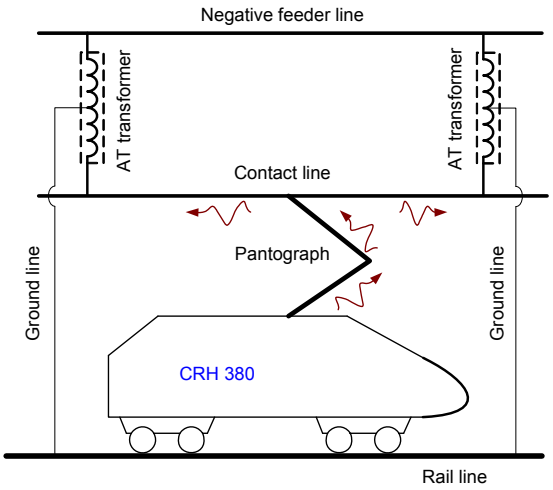

Fig. 1 Typical configuration used on the Beijing-Shanghai High-Speed Railway, China

An actual railway system is regarded as an assembly of uniform multiconductor transmission lines, which consists of catenary wire, contact wire, ground wire, negative feeder wire, and two rails. Multiconductor transmission lines structures are generally solved by the transmission line theory (Paul, 2008). In his classical book, all aspects about multiconductor transmission lines are considered. The drawback of transmission line theory is that only quasi-transverse electromagnetic (TEM) mode is considered. However, when the frequency becomes higher, other modes' influence will be enhanced. The mode analysis of an infinitely long line above the earth was first solved by Carson (1926). In his theory, the distributed parameters of a quasi-TEM transmission line were analyzed and calculated. Since then, many investigators have revisited the problem, and numerous studies have been carried out. Using Hertz potentials in three media, Sunde (1968) derived the results for a wider frequency range including the displacement currents in the soil, which was neglected in Carson (1926)'s model. Sunde (1968)'s model is suitable over wider frequency range. Excepting the quasi-TEM mode, other models that proved to be very important have been overlooked. Wait (1972) proposed a modal equation through a full-wave approach. The only approximations were thin-wire and complex exponential current-distribution. An extension of Wait (1972)'s model was provided by D'Amore and Starto (1996a; 1996b), pointing out that the transmission-line mode is dominant even when the quasi-TEM approximation does not hold. Kuester *et al.* (1978) and Olsen *et al.* (1978) proposed modal equation solutions including quasi-TEM mode, surface-attached mode, radiation mode, and surface wave. A good summary of this research can be found in (Olsen *et al.*, 2000). The line is assumed continuous in all the cases above.

But in fact the contact line is disconnected by an AT every 25 km, and a model considering the lumped-circuit is discussed in (Mazloom *et al.*, 2009). He composited the Finite Difference Time Domain (FDTD) routine and Alternative Transients Program (ATP), and proved that it was effective in dealing with the lumped components, such as boost transformers (BTs), ATs, track circuits, and line interconnections.

Under some condition, the disconnected wire can be seen as infinitely long (Cozza and Demoulin, 2008). Moreover, it is obvious that the overhead lines in a railway system are above the stratified earth, specially the rails above the sleeper. Thus, stratified earth has been investigated. The most influential research findings were summarized by Wait (1970) and Li (2009).

2 Magnetic field formulae

2.1 Geometry of railway system

The typical configuration of the multiconductor transmission lines system under consideration is shown in Fig. 2. R1 and R2 are the rails, whose cross-section is not presented realistically. The distance between them is 1435 mm, and track circuits are connected with them to ensure safety. R3 and R4 are,

respectively, a catenary wire and contact wire 6 m above the rails, connected by droppers in order to assure equipotential along the overhead line. R5 is a negative feeder wire connected to one end of the AT. R6 is a ground wire, one end of which is connected to the middle of the AT, and the other connected to the rail. Regions 0, 1 and 2 are the air, the middle layer, and the earth, respectively, characterized by μ_j, ε_j, σ_j, j=0, 1, 2, where μ_0 and ε_0 are respectively permeability and permittivity of vacuum, and σ_j is the conductivity of media i.

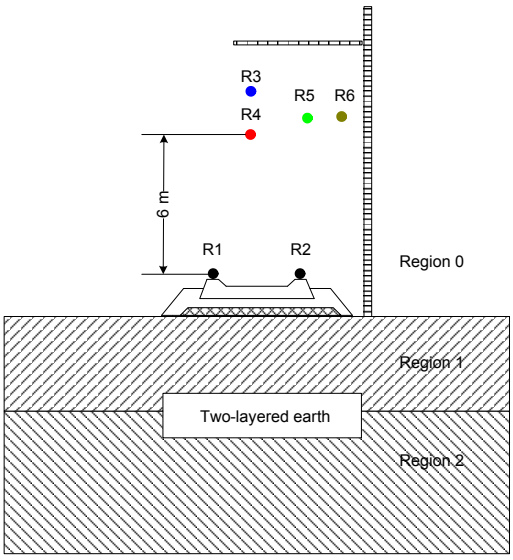

Fig. 2 Cross-section of the multiconductor lines under consideration

2.2 Integrated formulae

The wave numbers in the three-layered region are

$$k_0 = \omega\sqrt{\mu_0\varepsilon_0}, \tag{1}$$

$$k_j = \omega\sqrt{\mu_0\left(\varepsilon_0\varepsilon_{rj} + \mathrm{i}\sigma_j/\omega\right)}, \quad j = 1,2, \tag{2}$$

where ω is the angular speed, ε_{rj} is the relative dielectric constant of media j and $\mathrm{e}^{-\mathrm{i}\omega t}$ is used, the integrated formulae of the magnetic field in the air radiated by a horizontal infinitely long wire over a two-layered earth are (Wait, 1970)

$$B_{0x}(x,y,z) = \frac{I\mu_0}{4\pi}\left(B_{0x}^1 + B_{0x}^2 + B_{0x}^3\right), \tag{3}$$

$$B_{0z}(x,y,z) = \frac{I\mu_0}{4\pi}\left(B_{0z}^1 + B_{0z}^2 + B_{0z}^3\right), \tag{4}$$

where B^1 and B^2 are direct wave and ideal reflected wave,

$$B_{0x}^1 = \int_{-\infty}^{+\infty} \mathrm{e}^{\pm\mathrm{i}\gamma_0|z-d|}\mathrm{e}^{\mathrm{i}\lambda x}\mathrm{d}\lambda = \frac{2\mathrm{i}k_0(z-d)}{\sqrt{x^2+(z-d)^2}} K_1\left[\mathrm{i}k_0\sqrt{x^2+(z-d)^2}\right], \tag{5}$$

$$B_{0x}^2 = \int_{-\infty}^{+\infty} \mathrm{e}^{\mathrm{i}\gamma_0(z+d)}\mathrm{e}^{\mathrm{i}\lambda x}\mathrm{d}\lambda = \frac{2\mathrm{i}k_0(z+d)}{\sqrt{x^2+(z+d)^2}} K_1\left[\mathrm{i}k_0\sqrt{x^2+(z+d)^2}\right], \tag{6}$$

$$B_{0z}^1 = -\int_{-\infty}^{+\infty} \mathrm{e}^{\pm\mathrm{i}\gamma_0|z-d|}\mathrm{e}^{\mathrm{i}\lambda x}\frac{\lambda}{\gamma_0}\mathrm{d}\lambda = \frac{2\mathrm{i}k_0 x}{\sqrt{x^2+(z-d)^2}} K_1\left[\mathrm{i}k_0\sqrt{x^2+(z-d)^2}\right], \tag{7}$$

$$B_{0z}^2 = \int_{-\infty}^{+\infty} \mathrm{e}^{\pm\mathrm{i}\gamma_0(z+d)}\mathrm{e}^{\mathrm{i}\lambda x}\frac{\lambda}{\gamma_0}\mathrm{d}\lambda = -\frac{2\mathrm{i}k_0 x}{\sqrt{x^2+(z+d)^2}} K_1\left[\mathrm{i}k_0\sqrt{x^2+(z+d)^2}\right], \tag{8}$$

where d is the height of line source to the ground surface, and K_0 and K_1 are the modified Bessel functions.

$$B_{0x}^3 = \int_{-\infty}^{+\infty} \mathrm{e}^{\mathrm{i}\gamma_0(z+d)}\mathrm{e}^{\mathrm{i}\lambda x}(Q-1)\mathrm{d}\lambda, \tag{9}$$

$$B_{0z}^3 = \int_{-\infty}^{+\infty} \frac{\lambda}{\gamma_0}\mathrm{e}^{\mathrm{i}\gamma_0(z+d)}\mathrm{e}^{\mathrm{i}\lambda x}(Q-1)\mathrm{d}\lambda, \tag{10}$$

where

$$Q-1 = 2\frac{-\gamma_0\gamma_1 + \mathrm{i}\gamma_0\gamma_2\tan(\gamma_1 l)}{\gamma_0\gamma_1 + \gamma_1\gamma_2 - \mathrm{i}(\gamma_1^2 + \gamma_0\gamma_2)\tan(\gamma_1 l)}, \tag{11}$$

$$\gamma_j = \sqrt{k_j^2 - \lambda^2}, \quad j = 0,1,2, \tag{12}$$

where l is the thickness of middle layer.

The main aim is to evaluate the integrals using analytical techniques. Contour integral technique is applied to the above integrals. The contribution of residue to the integrals is called trapped surface wave, and the contribution of the integral along the branch lines is called the lateral wave. The complete wave contributions are provided next.

2.3 Trapped surface wave

From the above derivations, we know that the trapped surface wave is from the residue. The two factors of the residue are poles and expressions. First let us examine the pole equation:

$$\gamma_0\gamma_1+\gamma_1\gamma_2-i(\gamma_1^2+\gamma_0\gamma_2)\tan(\gamma_1 l)=0. \tag{13}$$

The roots are obtained using Newton's iteration method from the pole equation (Zhi *et al*., 2011).

Note that when the roots of the pole equation are solved, the residue is obtained easily. The terms of the trapped surface wave can be achieved as

$$B_{0x}^{\mathrm{S}}=-\mathrm{i}\mu_0 I\sum_j \mathrm{e}^{\mathrm{i}x\lambda_j^*+\mathrm{i}\gamma_0(\lambda_j^*)(z+d)} \times\frac{-\gamma_0(\lambda_j^*)\gamma_1(\lambda_j^*)+\mathrm{i}\gamma_0(\lambda_j^*)\gamma_2(\lambda_j^*)\tan\gamma_1(\lambda_j^*)l}{\gamma_1(\lambda_j^*)q'(\lambda_j^*)}, \tag{14}$$

$$B_{0z}^{\mathrm{S}}=\mathrm{i}\mu_0 I\sum_j \lambda_j^*\mathrm{e}^{\mathrm{i}x\lambda_j^*+\mathrm{i}\gamma_0(\lambda_j^*)(z+d)} \times\frac{-\gamma_0(\lambda_j^*)\gamma_1(\lambda_j^*)+\mathrm{i}\gamma_0(\lambda_j^*)\gamma_2(\lambda_j^*)\tan\gamma_1(\lambda_j^*)l}{\gamma_0(\lambda_j^*)\gamma_1(\lambda_j^*)q'(\lambda_j^*)}, \tag{15}$$

where

$$\begin{aligned}q'(\lambda)=&-\lambda\left(\frac{\gamma_0}{\gamma_1}+\frac{\gamma_1}{\gamma_0}+\frac{\gamma_2}{\gamma_1}+\frac{\gamma_1}{\gamma_2}\right)\\&+\mathrm{i}\lambda\tan(\gamma_1 l)\left(\frac{\gamma_0}{\gamma_2}+\frac{\gamma_2}{\gamma_0}+2\right)\\&+\mathrm{i}\sec^2(\gamma_1 l)\left(\gamma_1^2+\gamma_0\gamma_2\right)\frac{l\lambda}{\gamma_1}.\end{aligned} \tag{16}$$

2.4 Lateral wave

From the above derivations, we know that the lateral wave is from the integral along the branch lines. Fig. 3 shows that there are three branch lines, thus lateral wave consists of three compositions. The evaluation of the integral along the branch cut Γ_1 is zero and the integral along the branch cut Γ_2 can be neglected (Li, 2009). Thus, the lateral wave is mainly the contribution of branch cut Γ_0, which is presented in Eq. (A2) in the APPENDIX.

2.5 Final formulae for the magnetic field

Based on the above results, the final formulae of the magnetic fields B_{0x} and B_{0z} are shown in the APPENDIX, where

$$\begin{aligned}A&=-1+\mathrm{i}\frac{\gamma_0}{\gamma_1}\tan(\gamma_1 l)\\&\approx-1+\mathrm{i}\frac{\sqrt{k_2^2-k_0^2}}{\sqrt{k_1^2-k_0^2}}\tan\left(\sqrt{k_1^2-k_0^2}\,l\right),\end{aligned} \tag{17}$$

$$\begin{aligned}B&=\gamma_2-\mathrm{i}\gamma_1\tan(\gamma_1 l)\\&\approx-\sqrt{k_2^2-k_0^2}+\mathrm{i}\sqrt{k_1^2-k_0^2}\,\tan\left(\sqrt{k_1^2-k_0^2}\,l\right),\end{aligned} \tag{18}$$

$$\Delta=\frac{1}{\sqrt{2}}\left(\frac{B}{Ak_0}-\mathrm{i}\frac{z+d}{x}\right), \tag{19}$$

$$p^*=k_0 x\Delta^2. \tag{20}$$

It is seen that the total field is composed of the direct wave, the ideal reflected wave or image wave, the trapped surface wave, and the lateral wave.

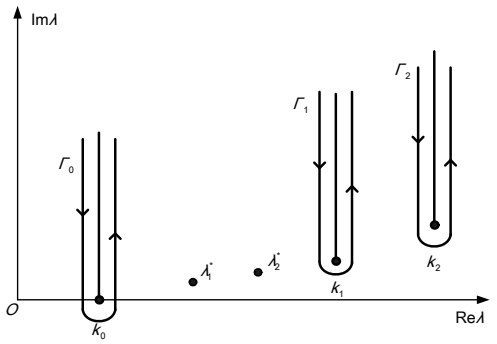

Fig. 3 Configuration of poles and branch lines

3 Computation results and comparation

With the measuring point on the interface z=0 m and the height of the source line d=6 m, ε_1=2.65, ε_2=8, σ_2=0.4 S/m, and f=10 MHz, 50 MHz and 500 MHz according to (CENELEC Standard EN50121, 2006) are considered for contact line. Magnitudes of the total field, the trapped surface wave, and DRL wave, which is composed of the direct wave, the ideal reflected wave, and the lateral wave, are computed at $k_1 l$=2.97π as shown in Figs. 4a–4c.

With the measuring point on the interface z=0 m and the height of the source line d=0.2 m, ε_1=2.65, ε_2=8, σ_2=0.4 S/m, and f=10 MHz, 50 MHz and 500 MHz are considered for rail line. Magnitudes of the total field, the trapped surface wave, and the DRL waves are computed at k_1l=2.97π as shown in Figs. 5a–5c.

Compared with trapped surface wave by a dipole in (Li, 2009), the amplitude of the trapped surface wave by a horizontal infinitely long wire has no dispersion losses, due to the wavefront of the trapped surface wave radiated over the two-layered earth is always a plane. This characteristic is different from that of a dipole source in the presence of a three-layered region. In the case of a dipole source, the wavefront is enlarged as the dispersion of the trapped surface, the amplitude of the trapped surface wave is attenuated as $\rho^{-1/2}$ in the ρ direction. The attenuation of trapped surface wave in all the figures is mainly due to the dielectric losses. And the nearer the observer is to the interface, the more important the strapped surface wave is when considering the thickness of the middle layer.

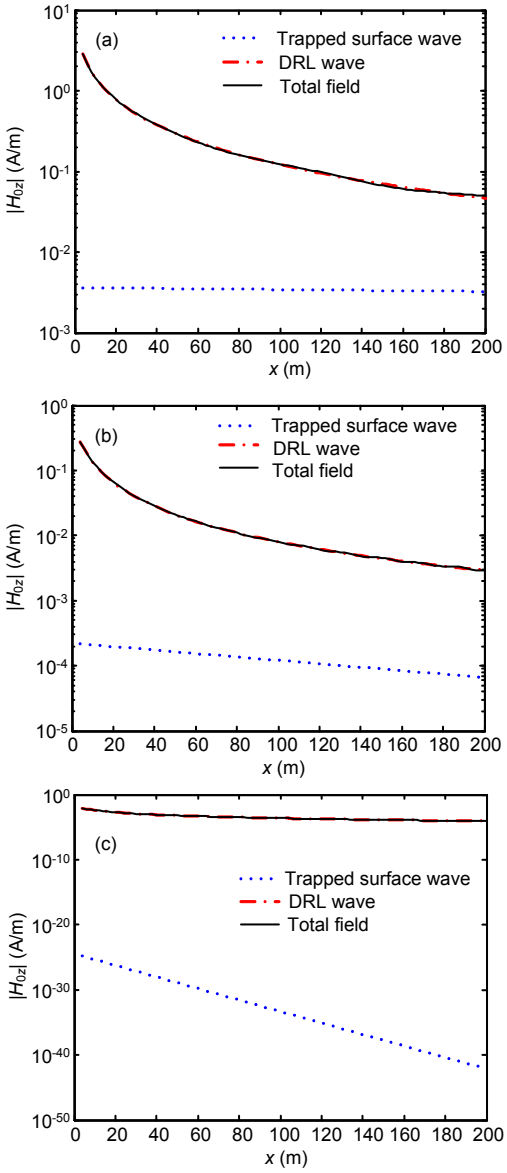

Fig. 4 Magnitude of H_{0z} vs propagating distances at z=0, d=6 m with ε_1=2.65, ε_2=8, σ_2=0.4 S/m and k_1l=2.97π
(a) f=10 MHz; (b) f=50 MHz; (c) f=500 MHz

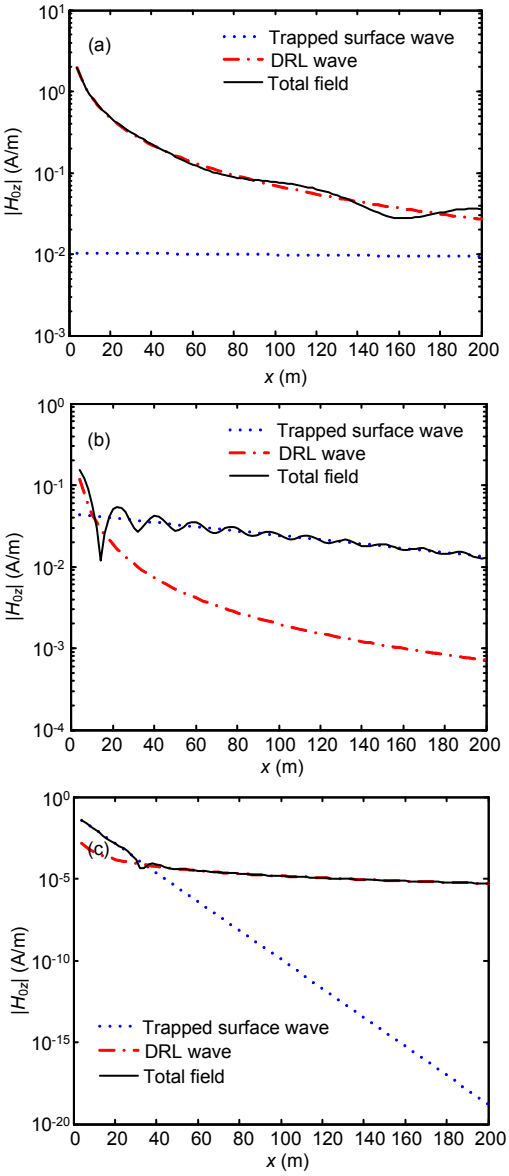

Fig. 5 Magnitude of H_{0z} vs propagating distances at z=0, d=0.2 m with ε_1=2.65, ε_2=8, σ_2=0.4 S/m and k_1l=2.97π
(a) f=10 MHz; (b) f=50 MHz; (c) f=500 MHz

4 Conclusions

Overhead lines in high-speed railway consist of catenary wire, contact wire, negative feeder wire, ground wire, and rails, which constitute multiconductor transmission lines. These lines are divided into two groups: contact lines and rail lines. Magnetic field around the lines is discussed as single line for contact lines and rail lines.

The total magnetic field consists of the direct wave, the ideal reflected wave or image wave, the trapped surface wave, and the lateral wave. The trend of the field and wave is attenuated along the x direction.

When the frequency becomes higher and the source is near the interface, the trapped surface wave is dominant. But when the source is away from the interface, the total field is dominated by DRL waves.

References

Carson, J.R., 1926. Wave propagation in overhead wires with ground return. *Bell System Technology Journal*, p.539-554.

CENELEC Standard EN 50121, 2006. Railway Applications-Electromagnetic Compatibility. European Committee for Electrotechnical Standardization.

Cozza, A., Demoulin, B., 2008. On the modeling of electric railway lines for the assessment of infrastructure impact in radiated emission tests of rolling stock. *IEEE Transactions on Electromagnetic Compatibility*, **50**(3):566-576. [doi:10.1109/TEMC.2008.924387]

D'Amore, M., Starto, M.S., 1996a. Simulation models of a dissipative transmission line above a lossy ground for a wide frequency range-Part I: Single conductor configuration. *IEEE Transactions on Electromagnetic Compatibility*, **38**(2):127-138. [doi:10.1109/15.494615]

D'Amore, M., Starto, M.S., 1996b. Simulation models of a dissipative transmission line above a lossy ground for a wide frequency range-Part II: Multiconductor configuration. *IEEE Transactions on Electromagnetic Compatibility*, **38**(2):139-149. [doi:10.1109/15.494616]

GB/T 24338-2009. Railway Applications-Electromagnetic Compatibility-Part 1: General. CSR Zhuzhou Times Electric Co., Ltd., CSR Qingdao Sifang Co., Ltd., and China Railway Electrification Survey Design & Research Institute Co. Ltd.

Kuester, E.F., Chang, D.C., Olsen, R.G., 1978. Modal theory of long horizontal wire structures above the earth, 1, excitation. *Radio Science*, **13**(4):605-613. [doi:10.1029/RS013i004p00605]

Li, K., 2009. Electromagnetic Fields in Stratified Media. Zhejiang University Press and Springer.

Mazloom, Z., Theethayi, N., Thottappillil, R., 2009. A method for interfacing lumped-circuit models and transmission-line system models with application to railways. *IEEE Transactions on Electromagnetic Compatibility*, **51**(3):833-841. [doi:10.1109/TEMC.2009.2023112]

Olsen, R.G., Kuester, E.F., Chang, D.C., 1978. Modal theory of long horizontal wire structures above the earth, 2, properties of discrete modes. *Radio Science*, **13**(4):615-623. [doi:10.1029/RS013i004p00615]

Olsen, R.G., Young, J.L., Chang, D.C., 2000. Electromagnetic wave propagation on a thin wire above earth. *IEEE Transactions on Antennas and Propagation*, **48**(9):1413-1419. [doi:10.1109/8.898775]

Paul, C.R., 2008. Analysis of Multiconductor Transmission Lines. John Wiley and Sons Press, New York, Chichester, Brisbane, Toronto, Singapore.

Sunde, E.D., 1968. Earth Conduction Effects in Transmission Systems. Dover, New York.

Wait, J.R., 1970. Electromagnetic Waves in Stratified Media (2nd Ed.). Pergamon Press, Oxford, London, New York, Paris.

Wait, J.R., 1972. Theory of wave propagation along a thin wire parallel to an interface. *Radio Science*, **7**(6):675-679. [doi:10.1029/RS007i006p00675]

Zhi, Y.J., Li, K., Fang, Y.T., 2011. Electromagnetic field of a horizontal infinitely long wire over the dielectric-coated earth. *IEEE Transactions on Antennas and Propagation*, in press. [doi:10.1109/TAP.2011.2167917]

APPENDIX

$$
\begin{aligned}
B_{0x} = & -\frac{\mathrm{i}I\mu_0 k_0 (z-d)}{2\pi\sqrt{x^2+(z-d)^2}} K_1\left[\mathrm{i}k_0\sqrt{x^2+(z-d)^2}\right] \\
& + \frac{\mathrm{i}I\mu_0 k_0 (z+d)}{2\pi\sqrt{x^2+(z+d)^2}} K_1\left[\mathrm{i}k_0\sqrt{x^2+(z+d)^2}\right] \\
& - \mathrm{i}\mu_0 I \sum_j \mathrm{e}^{\mathrm{i}x\lambda_j^* + \mathrm{i}\gamma_0(\lambda_j^*)(z+d)} \frac{-\gamma_0(\lambda_j^*)\gamma_1(\lambda_j^*) + \mathrm{i}\gamma_0(\lambda_j^*)\gamma_2(\lambda_j^*)\tan\gamma_1(\lambda_j^*)l}{\gamma_1(\lambda_j^*)q'(\lambda_j^*)} \\
& + \sqrt{2}\frac{I\mu_0}{4\pi}\left[\frac{B}{A}\mathrm{e}^{\mathrm{i}0.75\pi + \mathrm{i}k_0 x - \mathrm{i}\frac{k_0(z+d)^2}{2x}} \sqrt{\frac{\pi}{k_0 x}} - \mathrm{i}\pi\frac{B^2}{A^2 k_0}\mathrm{e}^{\mathrm{i}k_0 x - \mathrm{i}0.75\pi - \mathrm{i}\frac{k_0(z+d)^2}{2x} - \mathrm{i}k_0 x A^2} F(p^*)\right],
\end{aligned}
\tag{A1}
$$

$$
\begin{aligned}
B_{0z} = &+\frac{\mathrm{i}I\mu_0 k_0(z-d)}{2\pi\sqrt{x^2+(z-d)^2}}K_1\left[\mathrm{i}k_0\sqrt{x^2+(z-d)^2}\right]\\
&-\frac{\mathrm{i}I\mu_0 k_0(z+d)}{2\pi\sqrt{x^2+(z+d)^2}}K_1\left[\mathrm{i}k_0\sqrt{x^2+(z+d)^2}\right]\\
&+\mathrm{i}\mu_0 I\sum_j \mathrm{e}^{\mathrm{i}x\lambda_j^*+\mathrm{i}\gamma_0(\lambda_j^*)(z+d)}\lambda_j^*\frac{-\gamma_0(\lambda_j^*)\gamma_1(\lambda_j^*)+\mathrm{i}\gamma_0(\lambda_j^*)\gamma_2(\lambda_j^*)\tan\gamma_1(\lambda_j^*)l}{\gamma_0(\lambda_j^*)\gamma_1(\lambda_j^*)q'(\lambda_j^*)}\\
&+\sqrt{2}\frac{I\mu_0}{4\pi}\left[k_0\mathrm{e}^{\mathrm{i}0.75\pi+\mathrm{i}k_0x-\mathrm{i}\frac{k_0(z+d)^2}{2x}}\sqrt{\frac{\pi}{k_0.x}}-\mathrm{i}\pi\frac{B}{A}\mathrm{e}^{\mathrm{i}k_0x-\mathrm{i}0.75\pi-\mathrm{i}\frac{k_0(z+d)^2}{2x}-\mathrm{i}k_0x\Delta^2}F(p^*)\right].
\end{aligned}
\tag{A2}
$$